

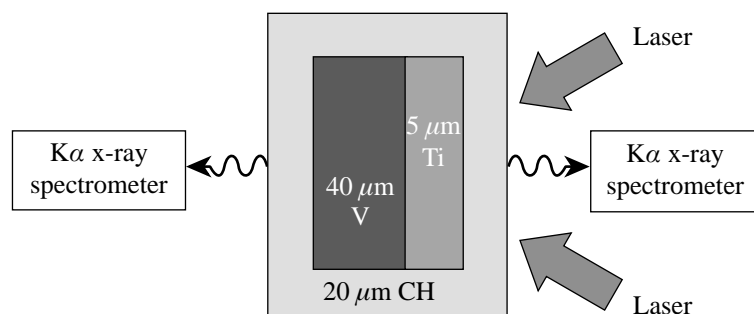
# Measurement of Preheat due to Fast Electrons in Laser Implosions

## Introduction

Fast electrons due to the two-plasmon-decay (2PD) instability have been measured in previous laser-interaction experiments.<sup>1,2</sup> The main impact of these electrons in laser-fusion experiments is the possible preheat that can reduce the implosion's effectiveness. The preheat caused by these electrons is studied by measuring the  $K\alpha$  line emission from high-Z layers in a flat-target geometry on the OMEGA<sup>3</sup> laser system. The  $K\alpha$  emission is directly related to the preheat level;<sup>4,5</sup> for sufficiently high fast-electron temperatures ( $T_{\text{fast}}$ ) the relationship between the  $K\alpha$  intensity and the preheat level is independent of  $T_{\text{fast}}$ . The preheat due to fast electrons in UV laser irradiation is relatively small and is usually masked by the preheat due to radiation. To overcome this problem, a target containing titanium (Ti) and vanadium (V) layers was designed so that when irradiated from the Ti side, most of the Ti- $K\alpha$  is excited by radiation, whereas most of the V- $K\alpha$  is excited by the fast electrons. As seen below, the thick Ti and V layers required for the  $K\alpha$  measurement precluded conducting this experiment in spherical geometry. We show, however, that such measurements can be used as a reference point for hard x-ray continuum detectors, which can then be used to determine the preheat in undoped spherical targets. The  $K\alpha$  measurements can conveniently be used as a reference point because in the case of x-ray continuum measurements  $T_{\text{fast}}$  must be known to determine the preheat level even at high temperatures.

## Flat-Target Experimental Configuration

The configuration for the flat-target experiment is shown in Fig. 82.19. Ten OMEGA beams of 1-ns square pulse duration and 4.85-kJ total energy are overlapped to yield a target irradiance of  $1.5 \times 10^{15}$  W/cm<sup>2</sup>. This value exceeds the irradiance in spherical implosion experiments on OMEGA, thus providing an upper limit on preheat in future experiments. The target consists of two main layers: 5- $\mu\text{m}$ -thick titanium and 40- $\mu\text{m}$ -thick vanadium. The 20- $\mu\text{m}$ -thick CH overcoat precludes any direct laser irradiation or heating of either metal, thus restricting laser interaction with the metals to preheat only. Indeed, the only lines seen in the measured spectra are the Ti- and V- $K\alpha$  lines. Two time-integrating x-ray spectrometers observe the spectrum emitted from the front side and the back side of the target. The purpose of the two-layer target is to ensure that most of the V- $K\alpha$  line is excited by fast electrons, not radiation. The Ti layer is thick enough to strongly absorb radiation above the Ti-K edge, thus minimizing the radiative excitation of  $K\alpha$  in the vanadium. To further increase the emission of the V- $K\alpha$  line due to fast electrons, the V-layer thickness should be made about equal to the range of fast electrons. Analysis of the  $K\alpha$  line intensities indicates, as seen below, a fast-electron temperature exceeding  $\sim 50$  keV. The range in vanadium can be well approximated<sup>6</sup> by the relation  $R(\text{g/cm}^2) = 9.4 \times 10^{-6} E^{5/3}$ , where  $E$  is the electron energy in keV. Thus the range of the fast electrons in vanadium is a few tens of microns. The  $(1/e)$  attenuation length of the V- $K\alpha$  line



E10228b

Figure 82.19

Experimental configuration for measuring fast-electron preheat. Ten incident laser beams are absorbed in the CH layer. Radiation excites the Ti- $K\alpha$  line, but most of it is absorbed before reaching the vanadium layer. On the other hand, fast electrons can penetrate the vanadium layer and excite the V- $K\alpha$  line.

in vanadium, however, is  $\sim 18 \mu\text{m}$ ; thus the vanadium layer should not be significantly thicker than  $\sim 18 \mu\text{m}$ , hence the choice of  $\sim 40 \mu\text{m}$ . Vanadium was chosen because the  $K\alpha$  lines of Ti and V are close enough to be simultaneously observed in the spectrum. Also, the back-layer material should have the higher  $Z$  of the two; otherwise, radiation of energy between the Ti- $K$  edge (4.96 keV) and the V- $K$  edge (5.46 keV) will be transmitted through the front layer and will strongly contribute to  $K\alpha$  emission in the back layer, contrary to the main goal of the experiment. Two crystal spectrometers viewed the emitted spectrum from the front and back of the target. The crystal in the front spectrometer was Ge(1,1,1); the one in the back was ADP(1,0,1).

Figure 82.20 shows the observed spectra from the front side and the back side of the target for shot 18167.  $K\alpha$  lines of Ti and V are seen, as well as the continuum emitted from the interaction region in the CH coating. The absolute energy in the  $K\alpha$  lines, which is required to determine preheat, is based on the following calibrations: (a) for the Ge crystal, a calibration performed at LLE<sup>7</sup> that agrees very well with the Darwin–Prins model,<sup>8</sup> (b) for the ADP crystal, two consistent calibrations,<sup>9,10</sup> and (c) for the DEF film, published calibration,<sup>11</sup> for which the film processing procedure was closely followed here. It should be further noted that both crystal calibrations change very little over the energy range of primary interest here,  $\sim 4.5$  to 5 keV. The target is viewed through a 25- $\mu\text{m}$ -

wide slit, which provides a one-dimensional image of the target at each wavelength, from which the space-integrated emission is computed. The space-integrated emission is larger than the measured emission by approximately the factor  $d/[d(1+M^{-1})]$ , where  $D$  is the FWHM of the emission region,  $d$  is the slit width, and  $M$  is the magnification. The following three sections deal with the analysis of the flat-target experimental results.

### Analysis of $K\alpha$ Emission

To analyze the measured  $K\alpha$  lines we first calculate their excitation due to radiation alone. We use the measured continuum intensity (Fig. 82.20) that is emitted by the laser-interaction region in the CH and transport it through the Ti and V layers (absorption in the CH is negligibly small). Only radiation above the Ti- $K$  edge (4.96 keV) must be included to calculate the excitation of either  $K\alpha$  line. Using the known opacity of cold Ti or V per unit areal density,  $\tau(E)$ , we solve the radiation transport equation for the spectral intensity  $I(x,E)$  into  $2\pi$  solid angle:

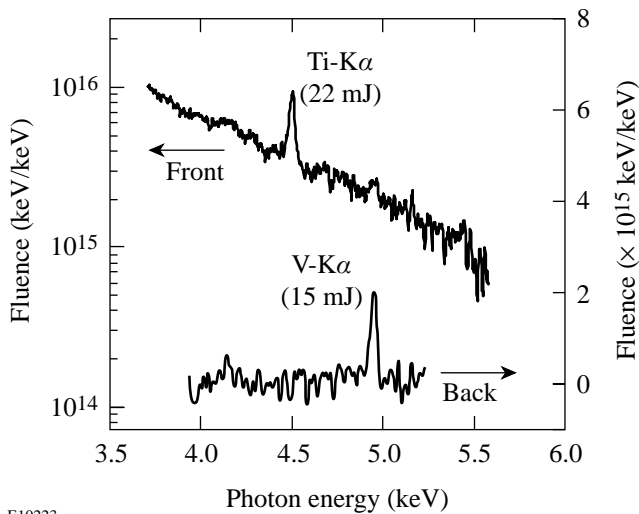
$$dI(x,E)/dx = -\tau(E)\rho I(x,E), \quad (1)$$

from which the local emission of Ti- $K\alpha$  is calculated according to

$$I(\text{Ti} - K\alpha) = E(K\alpha)\omega_K(\text{Ti})$$

$$\int_{E_K}^{\infty} I(x,E) \{1 - \exp[-\tau(\text{Ti})\rho\Delta x]\} dE/E, \quad (2)$$

and likewise for the V layer. Here  $\omega_K = 0.22$  is the fluorescence yield<sup>12</sup> of Ti, and  $E(K\alpha) = 4.508$  keV is the photon energy of the Ti- $K\alpha$  line; for V,  $\omega_K = 0.25$  and  $E(K\alpha) = 4.952$  keV. Using the normal density of the metal ( $\rho$ ) is justified since in plane geometry the areal density  $\rho\Delta x$  does not change when compression or expansion takes place. Also, shock arrival for most of the vanadium occurs after the laser pulse; thus, the preheating has been completed. The cold-metal opacity can be used since, as shown below, the degree of ionization due to the preheat is small (on average, two electrons per atom). Also, when removing the outer ( $M$ -shell) electrons, the  $K$  edge shifts very slightly to higher energies, but the absorption cross section at a given photon energy changes insignificantly.<sup>13</sup> The resulting spatial profiles of  $K\alpha$  emission, plotted in Fig. 82.21, show that some radiation survives

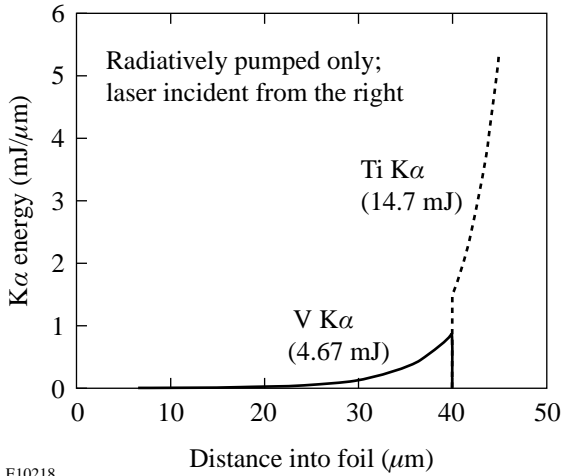


E10223

Figure 82.20

Time-integrated spectra emitted from the front and back of the target shown in Fig. 82.19. The measured line-intensity ratios are used to prove that the intensity of the V- $K\alpha$  line (observed from the back) is mostly due to fast electrons.

absorption in the titanium and excites V-K $\alpha$  near the V-Ti interface. The contribution of the observed K $\alpha$  lines is finally obtained by performing a radiation transport calculation of the K $\alpha$  line in both directions (exiting the target on the Ti side and on the V side, respectively). We now show that the results of these calculations disagree with the experiment, indicating that radiation alone cannot explain the measured intensity ratios, without the inclusion of fast-electron excitation of K $\alpha$ . For these considerations we use only line-intensity ratios, so the conclusion is independent of the accuracy in absolute calibration. Table 82.III compares the measured K $\alpha$  line-intensity ratios with the prediction of the radiative model, where front designates observation on the Ti (or laser side) and back designates observation on the V side of the target. The first measured ratio, V (back)/Ti (front), is much higher than predicted by the radiative model because fast electrons increase the V-K $\alpha$  intensity more than that of the Ti-K $\alpha$  intensity (because of the larger thickness of the former). Also, fast electrons excite V-K $\alpha$  throughout the vanadium layer rather than only near the V-Ti interface, thus reducing its attenuation when exiting on the V side. The same combination of effects explains the disagreement of the second ratio, V (back)/Ti (back). The third ratio, V (back)/V (front), is sensitive only to the spatial distribution of V-K $\alpha$  emission rather than to its origin. The disagreement in this case indicates that the V-K $\alpha$  line is emitted deeper into the vanadium and thus is attenuated less toward the back side, indicating again the contribution from long-range fast electrons.



E10218

Figure 82.21

Calculated spatial profiles of K $\alpha$  line emissions due only to radiation in the target of Fig. 82.19. The measured radiation from the interaction region (Fig. 82.20) was used as input.

Table 82.III: Comparison of radiative-model predictions and measurements.

K $\alpha$ -Line-Intensity Ratios	Radiative-Model Predictions	Measurements (Shot 18167)
V (back)/Ti (front)	0.05	~0.7
V (back)/Ti (back)	0.37	>>1
V (back)/V (front)	0.25	~5

We next analyze quantitatively the contribution of fast electrons to the K $\alpha$  line emission and show that the V-K $\alpha$  line viewed from the back is indeed excited mostly by fast electrons. We assume that the energies of fast electrons have a Maxwellian distribution (this assumption is based on 2-D simulations of the two-plasmon-decay instability<sup>14</sup>); the temperature and total energy of the fast electrons are considered free parameters in the calculation. A multigroup transport simulation of the electrons streaming through the Ti and V layers is performed, using the Bethe-Bloch slowing-down formula<sup>15</sup>

$$(-dE/dx)_{\text{coll}} = (2\pi e^4 N_a Z/E_0) \ln(1.16 E_0/\langle E_i \rangle), \quad (3)$$

where  $N_a$  is the atomic density,  $E_0$  the energy of the projectile electron, and  $\langle E_i \rangle$  the effective ionization energy.  $\langle E_i \rangle$  is determined by fitting Eq. (3) to experiments<sup>16</sup> using beam interaction with foil targets. For Ti,  $\langle E_i \rangle \sim 215$  eV, and for V,  $\langle E_i \rangle \sim 220$  eV. The validity of using this formula is discussed in Appendix A. The production of K $\alpha$  is calculated by the rate

$$dE(K\alpha)/dx = \sigma_K(E_v)(\rho/M_a)\omega_K(\text{Ti})E_K, \quad (4)$$

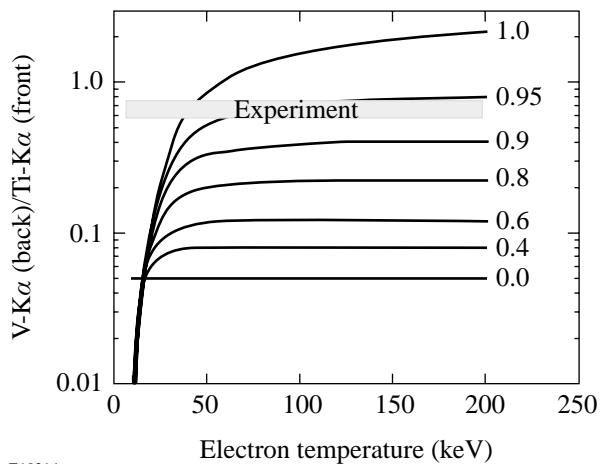
where the cross section is given by<sup>17</sup>

$$\sigma_K = (\pi e^4/E_v E_K) Z_K b_K \ln(c_K E_v/E_K), \quad (5)$$

where  $E_v$  is the photon energy,  $\rho$  is the mass density,  $M_a$  is the atomic mass,  $Z_K$  is the number of electrons in the  $K$  shell, and  $b_K$  and  $c_K$  are constants that change slowly with  $Z$ . By fitting Eq. (5) to detailed calculations,  $b_K$  and  $c_K$  have been determined for a wide range of elements. Even though Eq. (5) is nonrelativistic, the fitting was done for electron energies up to  $\sim 30$  times the  $K$ -edge energy, or  $\sim 160$  keV. Having determined thus the spatial distribution of K $\alpha$  line emission due to electrons, we transport the line intensity in both directions (as above) to calculate the contribution to the observed K $\alpha$  lines.

We finally add up the contributions from radiation and fast electrons and compare the calculated and measured  $K\alpha$  lines. As noted above, the calculated contribution of electrons depends on two free parameters (their temperature and total energy), whereas the contribution of radiation is calculated directly from the observed spectrum.

Figure 82.22 shows the results of the calculations for the ratio V (back)/Ti (front) as a function of the assumed electron temperature. The parameter for each curve is related to the assumed total energy in fast electrons. It is expressed as the fractional contribution of fast electrons to the V- $K\alpha$  (back) emission intensity. The experimental value of the V- $K\alpha$ (back)/Ti- $K\alpha$  (front) ratio,  $0.7\pm 0.1$ , is shown as a gray band in Fig. 82.22. The line marked 0.0 corresponds to removing the fast-electron component, whereas the curve marked 1.0 corresponds to removing the radiation component. In the limit of very high fast-electron temperatures (where the production of  $K\alpha$  lines by fast electrons is uniform over the target volume) the latter curve approaches the value  $\sim 2.3$ . This is smaller than the ratio 8 of V and Ti thicknesses because of the larger attenuation of the back-emergent V- $K\alpha$  line as compared with the front-emergent Ti- $K\alpha$  line. At low temperatures the electrons barely penetrate the Ti layer, and the V- $K\alpha$  line drops sharply. Comparing the curves in Fig. 82.22 with the experimental value indicates that *the electron temperature is higher*



E10214

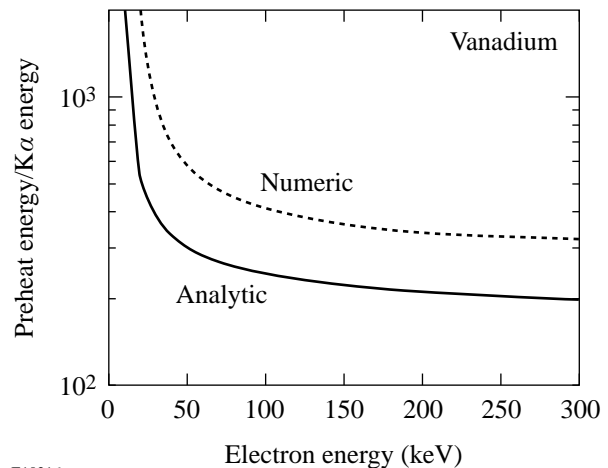
Figure 82.22

Calculated and measured ratio of V- $K\alpha$  observed from the back to Ti- $K\alpha$  observed from the front of the target due to both radiation and fast electrons. The parameter for each curve is the fraction of the V- $K\alpha$  line that is excited by electrons. Comparison with the experimental value of this ratio shows that (a) the V- $K\alpha$  line is excited almost exclusively by fast electrons, and (b) the temperature of fast electrons is  $\geq 50$  keV.

than  $\sim 50$  keV. For lower electron temperatures the V- $K\alpha$  line cannot be excited appreciably, and any excitation will be close to the Ti-V interface and be severely attenuated toward the back. Additional determinations of the fast-electron temperature will be described in the following sections. The primary conclusion from Fig. 82.22 is that *almost all of the intensity of the V- $K\alpha$  line (viewed from the back) is due to electron excitation*. This observable will now be used to estimate the preheat due to fast electrons.

### Determination of Electron Preheat from $K\alpha$ Measurements

In this section we discuss the determination of preheat level by fast electrons, using the  $K\alpha$  emission from the vanadium layer; preheat level as determined by hard x-ray emission will be the subject of the subsequent section. By dividing Eq. (3) by Eq. (4) we obtain the ratio of preheat to electron production of  $K\alpha$  lines. The result for V is shown as the curve marked *analytic* in Fig. 82.23. This curve tacitly assumes that the fast electrons are mono-energetic and the target is much thinner than the attenuation length. To remove these assumptions, we used the multigroup transport simulation described above to calculate the attenuation and  $K\alpha$  production of a Maxwellian distribution of electrons moving through the actual target used in this experiment. This calculation accounts for the distortion of the original Maxwellian distribution during transport



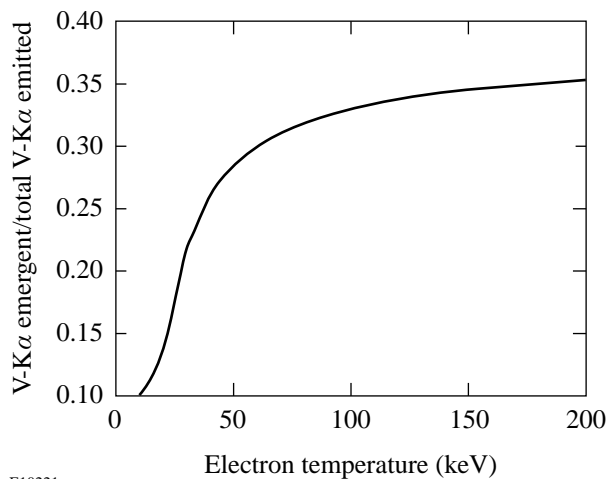
E10216

Figure 82.23

Determination of preheat from the measured V- $K\alpha$  intensity (after correction for transport, using Fig. 82.24). The analytic curve is the ratio of the relevant rates per cm propagation, while the numeric curve is the result of multigroup calculation for an initially Maxwellian distribution transported through the target of Fig. 82.19; for the latter case the abscissa values refer to the temperature of the fast electrons.

through the foil. The ratio of the space-integrated preheat and  $K\alpha$  production is shown by the curve marked *numeric* in Fig. 82.23; the abscissa for this curve is now the temperature rather than the energy of the fast electrons. The numeric curve is higher than the analytic curve because the slowing-down gradually brings the electrons to energies where the preheat is more effective. Finally, by multiplying the measured  $K\alpha$  energy (in absolute magnitude) by the appropriate value of the numeric curve, the preheat energy deposited in the target can be determined. As seen in Fig. 82.23,  $T_{\text{fast}}$  need not be known accurately to determine the preheat, as long as it is higher than  $\sim 50$  keV; Fig. 82.22 indicates that this was indeed the case here. It should be noted that the  $K\alpha$  intensity for this curve refers to the total local emission of  $K\alpha$ , which must be deduced from the observed  $K\alpha$ . The relation between the two depends on the spatial distribution of  $K\alpha$ , which in turn depends on  $T_{\text{fast}}$ . Also, the  $K\alpha$  intensity for this curve refers to the fraction of  $K\alpha$  that is excited solely by electrons.

Starting with the 15-mJ observed energy of V- $K\alpha$  (back), we estimate the total local V- $K\alpha$  emission. In Fig. 82.24 we show the relationship between the two as a function of  $T_{\text{fast}}$ . For  $T_{\text{fast}}$  higher than  $\sim 50$  keV the ratio is  $\sim 0.35$ , yielding 39 mJ for the total emission of V- $K\alpha$ . From Fig. 82.23 this corresponds to a preheat in the V of  $\sim 12$  J. For the total Ti-V target the preheat is  $\sim 14$  J (an increase of approximately the ratio of thicknesses  $45 \mu\text{m}/40 \mu\text{m}$ ); thus the preheat energy is about 0.3% of the incident laser energy.



E10221

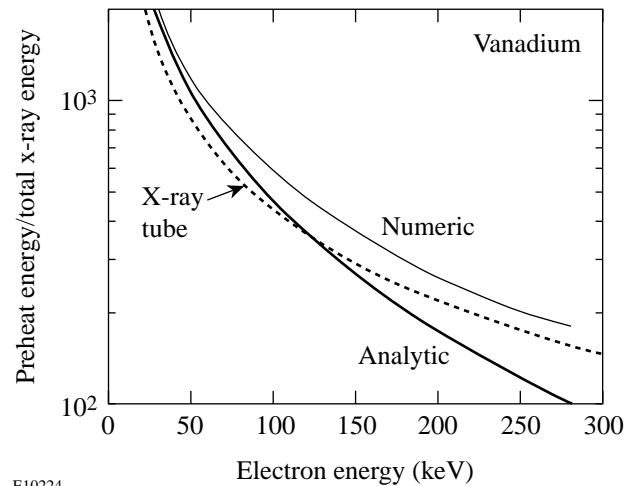
Figure 82.24  
Calculated ratio of V- $K\alpha$  energy emergent from the back of the target to the total volume emission of V- $K\alpha$ . The former quantity is the one measured, whereas the latter is used to derive the preheat.

### Determination of Electron Preheat from Hard X-Ray Measurements

In undoped targets, with no emission of  $K\alpha$  lines, preheat levels can be determined by measuring the spectrum of hard x-ray continuum. We show here that the spectrum-integrated x-ray continuum is directly related to the preheat deposited in the target, with no need to know the trajectories of the fast electrons in and around the target or the energy lost to the acceleration of ions. The loss rate due to bremsstrahlung is given by the Heitler relativistic formula<sup>18</sup>

$$\left(-dE/dx\right)_{\text{rad}} = N_a Z^2 \alpha \left(e^2/mc^2\right)^2 \left(E_0 + mc^2\right) \times \left\{4 \ln\left[2\left(E_0 + mc^2\right)/mc^2\right] - 4/3\right\}, \quad (6)$$

where  $N_a$  is the atomic density,  $\alpha$  is the fine-structure constant, and  $E_0$  is the energy of the projectile electron. It should be noted that, unlike for the collision loss rate, the relativistic formula yields considerably higher values than the classical formula (by a factor of  $\sim 2$  at 100 keV). Dividing Eq. (3) by Eq. (6) gives the ratio of preheat energy to radiation energy, shown by the curve marked *analytic* in Fig. 82.25. As in the equivalent case of  $K\alpha$  energy (Fig. 82.23) we use a multi-group electron transport calculation applied to the target in



E10224

Figure 82.25  
Determination of preheat from the spectrum-integrated hard x-ray emission. The analytic curve is the ratio of the relevant rates per cm propagation, while the numeric curve is the result of multigroup calculation for an initially Maxwellian distribution transported through the target of Fig. 82.19; for the latter case the abscissa values refer to the temperature of the fast electrons. The curve marked *x-ray tube* is the inverse of the empirical x-ray efficiency of a vanadium x-ray tube of an applied voltage  $E$ .

Fig. 82.19. The electrons are assumed to have a Maxwellian distribution of energies (rather than the same energy); the attenuation and distortion of the distribution during transport through the thick target are accounted for, and the ratio of space-integrated preheat and radiation is calculated. The result is marked *numeric* in Fig. 82.25, and for this curve the abscissa designates the temperature rather than the energy of the fast electrons. As in Fig. 82.23, the numeric curve is higher than the analytic curve; this is simply due to the rise of the curves in Fig. 82.25 for lower energies.

We can gain additional confidence in the curves in Fig. 82.25 by comparing them with the efficiency data of an x-ray tube with a vanadium anode. The input power that accelerates the electrons in the tube is converted mainly to heating the anode (equivalent to preheat in our case), with a fraction converted to x rays, mostly continuum. The power of x-ray continuum emission is given by<sup>19</sup>  $P = K(Z) \times Z \times I \times V^2$ , where  $V$  and  $I$  are the accelerating voltage and the tube current, respectively, and  $K$  depends weakly on  $Z$ . Thus, the ratio of preheat to radiation is  $\varepsilon = [Z \times V \times K(Z)]^{-1}$ . For vanadium, the empirical value<sup>19</sup> of  $K$  is  $\sim 1.1 \times 10^{-6} \text{ keV}^{-1}$ , resulting in the curve marked *x-ray tube* in Fig. 82.25 ( $V$  is the electron energy). Good agreement with the theoretical curves is seen.

#### ACKNOWLEDGMENT

Useful discussions with R. W. Short are gratefully acknowledged. This work was supported by the U.S. Department of Energy Office of Inertial Confinement Fusion under Cooperative Agreement No. DE-FC03-92SF19460, the University of Rochester, and the New York State Energy Research and Development Authority. The support of DOE does not constitute an endorsement by DOE of the views expressed in this article.

#### Appendix A: Slowing-Down Formulas for Partly Ionized Vanadium

The Bethe–Bloch slowing-down equation [Eq. (3)] applies to charged particles interacting with a cold, un-ionized target. In our case the vanadium layer is heated by fast electrons (and also by a shock wave) and is partly ionized. We examine here the required modifications to Eq. (3). We start by estimating the degree of ionization in the vanadium, based on the total target preheat energy estimated above. The total preheat derived from the  $K\alpha$  lines was 14 J. Dividing this energy by the preheated volume (given by the product of the focal-spot area and the target thickness), we derive a preheat per atom of  $E_a \sim 100$  eV. We estimate the temperature and average ionization consistent with  $E_a$  by solving the Saha equations of vanadium charge states and calculating  $E_a$  and  $\langle Z \rangle$  from

$$E_a = (3/2)[\langle Z \rangle + 1]kT_e + \sum_Z N_Z E_i(Z), \quad (\text{A1})$$

$$\langle Z \rangle = \sum_Z Z N_Z,$$

where  $N_Z$  is the relative population and  $E_i(Z)$  is the ionization energy of charge state  $Z$ . For any chosen value of the mass density  $\rho$  we find the  $N_e$  and  $T_e$  values that satisfy two conditions: (a) the calculated value of  $E_a$  from Eq. (A1) equals 100 eV and (b) the value of  $\langle Z \rangle$  calculated from Eq. (A1) agrees with  $N_e M_a / \rho$  ( $M_a$  is the atom mass). There is a unique solution consistent with both  $\rho$  and  $E_a$ . For mass densities in the range of 0.1 to 10 times the solid density of V, the resulting temperature varies from 18 to 43 eV and  $\langle Z \rangle$  varies from 1.4 to 2.6; therefore, only about 10% of the V and Ti electrons are ionized, whereas the rest remain bound. In calculating the slowing-down of the projectile electrons we must add the contributions of the bound electrons and the plasma (as shown below, the two are not totally independent). In justifying the approximations adopted below, we shall assume as typical parameter values an electron projectile energy of 50 keV moving through a solid-density vanadium plasma of temperature  $T_e = 30$  eV. Equation (3) plus the equations in this Appendix are valid for electrons that are fast but not highly relativistic. This means that the projectile electron velocity  $v$  must be much higher than a typical electron velocity in the medium but the relativistic quantity  $\gamma$  should not be much greater than 1. For a 50-keV-projectile electron, the velocity  $v_0 = 0.98 \times 10^{10}$  cm/s and  $\gamma \sim 1.1$ . For our case, the fully relativistic formula [Eq. (3) in Ref. 15] differs very little from Eq. (3) above; even at an electron projectile of 250 keV the two differ by only 1.5%. On the other hand,  $v_0$  is much larger than the thermal electron velocity in the medium ( $\sim 4 \times 10^8$  cm/s) and larger than the Fermi velocity

$$(3\pi^2 N_e)^{1/3} / (\hbar/m) \sim 2 \times 10^8 \text{ cm/s.}$$

The slowing-down of electrons due to a plasma can be divided into two contributions: binary collisions and collective collisions (i.e., excitation of plasma waves). In the kinetic formulations of the problem the division between the two regimes is marked by an impact parameter that is smaller or larger than the Debye length  $L_D$ . In the continuum (or dielectric) formulations of the problem the division is marked by a density-modulation wave number  $k$  that is larger or smaller than  $k_D = 1/L_D$ . The effect of plasma ions is negligible for the

high projectile velocities considered here.<sup>20</sup> The addition of the two electron collision terms for high projectile velocities yields<sup>20</sup>

$$(-dE/dx)_{\text{free}} = (2\pi e^4 N_{e,\text{free}}/E_0) \ln(1.52 E_0/\hbar\omega_p), \quad (\text{A2})$$

where  $\omega_p^2 = 4\pi e^2 N_{e,\text{free}}/m$ . It should be noted that the Debye length has cancelled out. This is because the argument of the logarithm in the binary-collision term is  $(L_D/1.47 b_{\text{min}})$ , where  $b$  is the impact parameter, whereas in the collective-collision term it is  $(1.123 v_0/\omega_p L_D)$ , where  $v_0$  is the projectile velocity; thus, by adding the two terms, the Debye length cancels out. This is an indication that the result is independent of the degree of degeneracy, which was also shown directly by Maynard and Deutsch.<sup>21</sup> For small degeneracy and high projectile velocity ( $v_0 \gg v_F$ ) the logarithm in Eq. (A2) is the first term in a series expansion where the second term is given by

$$(kT_e/E_F) \left[ I_{3/2}(\alpha)/I_{1/2}(\alpha) \right] (v_F/v_0)^2, \quad (\text{A3})$$

$I_{3/2}(\alpha)$  and  $I_{1/2}(\alpha)$  being the Fermi integrals. For our case  $(kT_e/E_F) \left[ I_{3/2}(\alpha)/I_{1/2}(\alpha) \right] \sim 1$ , but  $(v_F/v_0)^2 \sim 1.5 \times 10^{-3}$ , making the correction negligible. Likewise Yan *et al.*<sup>22</sup> have shown that when calculating the slowing-down for  $v_0/v_F \gg 1$ , the following effects can be neglected: electron degeneracy, strongly coupled plasma [in which case the random phase approximation implied in Eq. (A2) is invalid], and projectile collisions. In the derivation of Eq. (A3) the substitution  $b_{\text{min}} = \hbar/mv_0$  was made. This is the quantum limit (derived from the uncertainty principle) and is the relevant one for our case since it is a factor of  $\sim 58$  larger than the classical limit given by  $b_{\text{min}} = e^2/mv_0^2$ .

Before adding the relative contributions of free and bound electrons to the projectile slowing-down we modify Eq. (3) because of the Coulomb screening of the bound electrons by the free electrons.<sup>23</sup> In the derivation of Eq. (3) the maximum impact parameter is given by  $b_{\text{max}} \sim \hbar v_0/\langle E_i \rangle$ , where  $\langle E_i \rangle$  is the average ionization energy; however, for our typical values  $b_{\text{max}} \sim 2.5 \text{ \AA}$ , whereas the Debye length (calculated using  $N_{\text{free}}$ ) is  $\sim 1.5 \text{ \AA}$ . Therefore, we have to replace  $b_{\text{max}}$  by  $L_D$ , and Eq. (3) then becomes

$$(-dE/dx)_{\text{bound}} = (2\pi e^4 N_a Z/E_0) \times \ln \left[ (2E_0 kT_e)^{1/2} / \hbar\omega_p \right]. \quad (\text{A4})$$

Here  $\omega_p$  is given again in terms of the density of free electrons. It should be noted that the polarization of the vanadium ions by the projectile electrons and its effect on the slowing-down are significant only for  $\gamma \gg 1$  and can be ignored here.<sup>20</sup> The total slowing-down is given by the sum of Eqs. (A2) and (A4). For the typical conditions considered here the logarithm in Eq. (A2) equals  $\sim 8.2$ , and the logarithm in Eq. (A4) equals  $\sim 4.5$ . Since only  $\sim 10\%$  of the V electrons are free, the former must be multiplied by 0.1, yielding  $\sim 0.8$ . Finally, the sum  $4.5 + 0.8 = 5.3$  should be compared with the value of the logarithm in Eq. (3), which was used above to calculate the preheat, namely  $\sim 5.4$ . Therefore, the modified slowing-down formulation yields results that are essentially the same as those of Eq. (3), so the modifications to Eq. (3) can be neglected.

## REFERENCES

1. N. A. Ebrahim *et al.*, Phys. Rev. Lett. **45**, 1179 (1980); D. M. Villeneuve, R. L. Keck, B. B. Afeyan, W. Seka, and E. A. Williams, Phys. Fluids **27**, 721 (1984).
2. H. Figueroa *et al.*, Phys. Fluids **27**, 1887 (1984); T. A. Peyser *et al.*, Phys. Fluids B **3**, 1479 (1991).
3. T. R. Boehly, R. S. Craxton, T. H. Hinterman, J. H. Kelly, T. J. Kessler, S. A. Kumpan, S. A. Letzring, R. L. McCrory, S. F. B. Morse, W. Seka, S. Skupsky, J. M. Soures, and C. P. Verdon, Rev. Sci. Instrum. **66**, 508 (1995).
4. B. Yaakobi, I. Pelah, and J. Hoose, Phys. Rev. Lett. **37**, 836 (1976); J. D. Hares *et al.*, Phys. Rev. Lett. **42**, 1216 (1979).
5. A. Hauer, W. Priedhorsky, and D. van Hulsteyn, Appl. Opt. **20**, 3477 (1981).
6. M. J. Berger and S. M. Seltzer, Tables of Energy Losses and Ranges of Electrons and Positrons, NASA Document SP-3012, Washington, DC (1964).
7. See National Technical Information Service No. DE83015439 (A. J. Burek and B. Yaakobi, Final Report to the National Bureau of Standards Contract NB81NAHA2032, Appendix A, 1983). Copies may be ordered from the National Technical Information Service, Springfield, VA 22161.
8. B. L. Henke, E. M. Gullikson, and J. C. Davis, At. Data Nucl. Data Tables **54**, 181 (1993).
9. J. V. Gilfrich, D. B. Brown, and P. G. Burkhalter, Appl. Spectrosc. **29**, 322 (1975).
10. P. G. Burkhalter *et al.*, in *X-Ray Calibration: Techniques, Sources, and Detectors*, edited by P. Lee and P. D. Rockett (SPIE, Bellingham, WA, 1986), Vol. 689, pp. 121–127.
11. B. L. Henke *et al.*, J. Opt. Soc. Am. B **3**, 1540 (1986).
12. W. Bambynek *et al.*, Rev. Mod. Phys. **44**, 716 (1972).

13. D. J. Botto, J. McEnnan, and R. H. Pratt, *Phys. Rev. A* **18**, 580 (1978).
14. A. B. Langdon, B. F. Lasinski, and W. L. Kruer, *Phys. Rev. Lett.* **43**, 133 (1979).
15. G. Knop and W. Paul, in *Alpha-, Beta- and Gamma-Ray Spectroscopy*, 1st ed., edited by K. Siegbahn (North-Holland, Amsterdam, 1965), Chap. 1, Vol. 1, p. 12.
16. C. J. Bakker and E. Sergrè, *Phys. Rev.* **81**, 489 (1951); H. H. Andersen and J. F. Ziegler, *Hydrogen Stopping Powers and Ranges in All Elements, The Stopping and Ranges of Ions in Matter*, Vol. 3 (Pergamon Press, New York, 1977).
17. C. J. Powell, *Rev. Mod. Phys.* **48**, 33 (1976).
18. W. Heitler, *The Quantum Theory of Radiation*, 2nd ed., The International Series of Monographs on Physics (Oxford University Press, London, 1947).
19. N. A. Dyson, *X-Rays in Atomic and Nuclear Physics*, 2nd ed. (Cambridge University Press, Cambridge, England, 1990), p. 47.
20. J. D. Jackson, *Classical Electrodynamics*, 2nd ed. (Wiley, New York, 1962), Chap. 13.6.
21. G. Maynard and C. Deutsch, *Phys. Rev. A* **26**, 665 (1982).
22. X.-Z. Yan *et al.*, *Phys. Rev. A* **32**, 1785 (1985).
23. T. A. Mehlhorn, *J. Appl. Phys.* **52**, 6522 (1981).